Numerical Continuation of Periodic Orbits for Harmonically Forced Nonlinear Systems

Michael W. Sracic
Graduate Research Assistant, Ph.D Candidate
mwsracic@wisc.edu
&
Matthew S. Allen
Assistant Professor
msallen@engr.wisc.edu
Department of Engineering Physics
University of Wisconsin-Madison
534 Engineering Research Building
1500 Engineering Drive
Madison, WI 53706

ABSTRACT

A nonlinear structure will often respond periodically when it is excited with a sinusoidal force. Several methods are available that can compute the periodic response for various drive frequencies, which is analogous to the frequency response function for a linear system. The simplest approach would be to compute a sequence of simulations where the equations of motion are integrated until damping drives the system to steady state, but that approach suffers from a number of drawbacks. Recently, numerical methods have been proposed that use a solution branch continuation technique to find the free response of unforced, undamped nonlinear systems for different values of a control parameter. These are attractive because they are built around broadly applicable time-integration routines, so they are applicable to a wide range of systems. However, the continuation approach is not typically used to calculate the periodic response of a structural dynamic system to a harmonic force. This work adapts the numerical continuation approach to find the periodic, forced steady-state response of a nonlinear system. The method uses an adaptive procedure with a prediction step and a mode switching correction step based on Newton-Raphson methods. Once a branch of solutions has been computed, it explains how a full spectrum of harmonic forcing conditions affect the dynamic response of the nonlinear system. The approach is developed and applied to calculate nonlinear frequency response curves for a Duffing oscillator and a low order nonlinear cantilever beam.

1. Introduction

Many engineering structures exhibit nonlinear behavior. Some common examples include: shock absorbers in automotive suspension systems, bolted joints in aerospace structures and nonlinear elastic tissues in biomechanical systems. Nonlinearities can be due to geometric effects such as buckling, nonlinear constitutive relationships in materials, or dissipative effects such as the damping due to mechanical joints. The nonlinearities greatly affect the dynamic response of a structure and can lead to resonance phenomena that are not predicted by linear theory. One needs to accurately characterize the nonlinear dynamic response to accurately predict the structure's response and avoid structural failure.

Many nonlinear systems are operated under the presence of harmonic forcing that induces a periodic response. Some common examples of harmonically forced nonlinear systems include rotor systems with bearing nonlinearities [1-3], turbomachinery [4, 5], wind turbines [6], and nonlinear electrical circuits [7-9]. The response of the human musculoskeletal system is also highly nonlinear [10-13], and researchers often study neural network control systems as a form of oscillatory control force [14-17]. Even if a system does not naturally operate periodically under harmonic forcing, it is typical to perform experimental vibration testing using harmonic forcing (i.e. sine sweep testing) to better understand its behavior. Whenever a nonlinear system is harmonically forced, the specific forcing configuration can greatly affect the response of the system. For example, a nonlinear system that is excited with a sinusoid may respond harmonically at a number of

frequencies, and the dominant frequency could be different from the forcing frequency. In another case, there may be several possible periodic solutions (stable or unstable) for a single forcing function. For certain forcing configurations, the response of a highly nonlinear system may be approximately linear, while a weakly nonlinear system may exhibit strong nonlinearity. In order to fully understand the dynamics of a nonlinear structure, especially one that will be harmonically forced, it is important to predict and characterize the periodic responses that are produced by each forcing configuration.

Many techniques have been developed to calculate the periodic solutions of nonlinear systems, and those techniques usually take one of two basic approaches. The first approach is to approximate the analytical solution to the differential equations. The *harmonic balance technique*, which is similar to what is done for linear forced oscillations, is a popular approach where one assumes a harmonic series for the solution and usually truncates the series after one harmonic term [18, 19]. This approximate method tends to exhibit large error when the response contains strong higher harmonics; so additional terms can be included in the series, but this makes the mathematical formulation more difficult. The *method of multiple scales* and the *method of averaging* are commonly used perturbation techniques where one attempts to find an asymptotic linearization of the nonlinear solution, again using an approximating functional form for an analytical solution. A number of applications of these methods can be found in the following works [18, 20, 21]. All of these methods can provide accurate solutions in certain situations, but they can be difficult to implement for higher order systems that are strongly coupled, they are not straightforward to automate for a large range of forcing configurations, and they involve approximations so considerable expertise may be needed to be sure that those approximations are warranted. The second approach to calculating periodic solutions for nonlinear systems employs numerical methods. Essentially, one deals with the exact nonlinear equations for a system and uses direct time integration to search for the solution. This direct approach is powerful because closed form equations of motion are not required. If a system is damped then one can always calculate the periodic orbit conditions by integrating the equations of motion from a given set of initial conditions for a long enough time that the system settles into a steady periodic orbit. Typically, an adaptive time step control, fourth-order Runge-Kutta method [22, 23] or Newmark method [24] is used for time integration of structural dynamics systems. Although this approach is straightforward, it can be computationally expensive, and methods have been developed over the years to streamline such calculations. In fact, methods that find the periodic solutions of general differential equations are somewhat mature [25]. Two typical approaches are to evaluate and update a cost function with optimization [26, 27] or to solve a boundary value problem using a Newton-Raphson correction method [25]. The latter approach is widely used because the Newton-Raphson method converges quadratically. These approaches are usually started with an initial guess, which is subsequently corrected to satisfy convergence criteria, and this overall procedure is generally termed a *shooting* method. A parameter of interest can then be varied and the shooting method applied multiple times to compute a branch of solutions, and this is termed a *continuation* method. A general overview of shooting and continuation techniques is provided in [28].

Generally speaking, the methods for forced continuation can be categorized as corrector techniques, predictor-corrector techniques, or adaptive predictor-corrector techniques. Correction techniques use the general shooting technique to calculate solutions. Continuation is commonly performed with these methods by incrementing the forcing frequency (perhaps sequentially), using the previous solution as the initial conditions for the shooting method calculation of the solution. This procedure is improved by using a predictor-corrector algorithm, where each solution is used to calculate a prediction for the next solution on the curve. A prediction can be made for both the new forcing frequency and the new periodic response values. Then, the prediction is used as the initial guess for some form of shooting method that calculates the actual solution, and the convergence is usually much faster than without a prediction. Predictions can be made with a number of different geometric calculations, for example by calculating the tangent to the branch of solutions. More advanced methods will use an adaptive predictor-corrector algorithm, where the number of convergence calculations are recorded and used to adapt the prediction increment size between successive solutions, which further improves the efficiency of the calculations. A few well developed packages exist that use various forms of adaptive predictor-corrector methods for nonlinear system calculations. AUTO [29] is a code that is available for download. It has many sophisticated computational methods for nonlinear systems, but it does not contain a straightforward algorithm for calculating the periodic solutions of harmonically forced nonlinear systems. MATCONT [30] is another well developed package. It can be run in MATLAB and has a graphical user interface, but it is more suited towards calculating periodic solutions of autonomous systems. These codes are freely available for use but are not suited for all problems, so many researchers are still developing their own algorithms. A few of these use a simple corrector approach. In [31], a shooting method was applied to find periodic solutions of autonomous nonlinear systems. A single initial guess was used to calculate an entire branch of solutions for one parameter of interest, as opposed to performing some form of continuation from one solution to the next. In [23], a continuation method was used to calculate the forced-response periodic displacements of the center of a low-order model of a beam with clamped ends. A secant predictor step was used to vary the forcing frequency, but no predictions were calculated for the response solutions. The method showed promising results, but the algorithm could not follow sharp turns of the periodic solution branch. In [32], the harmonic balance method was used to calculate the periodic solutions of a reduced order torsional subsystem. Then, an

adaptive predictor continuation algorithm was used to find additional solutions as the operating frequency was varied. This method produced very detailed periodic solution curves but still requires one to use the approximations required by the harmonic balance method. If too few terms are used in the expansion then the algorithm may not predict important nonlinear features, as noted in [32]. A form of predictor-corrector continuation was also used in [22, 33-35]. They incremented the forcing frequency sequentially and then calculated a prediction for only the state vector with a first order Euler expansion from the previous solution. The algorithm provides quite robust performance. For example, in regions where a periodic solution branch has a turning point (i.e. a multiple solutions region), the algorithm included a re-parameterization of the solution curve in order to follow the turning point. The algorithm was applied to a few low order systems and showed promising results. More recently, a similar form of predictor-corrector continuation was presented in [24]. This method employs a *pseudo-arc length* continuation procedure that has a tangent predictor step and orthogonal corrector steps. Furthermore, the algorithm automatically controls the step size and exploits symmetry in the response to increase computational efficiency. So far, the authors of this method have computed the periodic solutions of a number of unforced, undamped nonlinear systems of high complexity and high order [24, 36-42] with exceptional detail. However, they have not extended their methods to the calculations of periodic solution branches of harmonically forced nonlinear systems.

The goal of this work is to create a continuation method for efficiently calculating the periodic solutions of harmonically forced nonlinear systems. This work will utilize techniques primarily from [24] in order to do this. A Newton-Raphson correction technique will be used to calculate the first solution from an initial guess that the user must supply. In order to calculate the subsequent solutions, an adaptive predictor step is used with a mode-switching correction step that employs two additional Newton-Raphson correction methods. The forcing frequency is the parameter that is varied. The most important difference of this work from the previous methods is that the prediction calculation and the Newton-Raphson correction methods includes extra terms that quantify how the periodic orbit varies as the forcing frequency is varied. Additionally, the forced periodic orbit is uniquely determined by the phase of the forcing, so the periodic orbits are calculated with respect to zero phase on the force, and since the frequency of the forcing is varied, the equations of motion change with each periodic orbit calculation; this is accounted for by the proposed method. The procedure of the proposed continuation method will first be outlined. Then, the shooting method and the Newton-Raphson correction method will be reviewed, and the necessary changes of those procedures due to the harmonic forcing will be derived. The continuation procedure will then be explained in detail. In Sections 3 and 4, the algorithm will be applied to calculate the periodic solutions of one and two degree of freedom systems, respectively. The results will be used to better understand the nonlinear systems, and discussion will be provided regarding the performance of the algorithm. Conclusions will be provided in Section 5.

2. Theory

A nonlinear system with input $u(t)$ can be described by the following state space differential equation

$$\dot{z} = f\left(z(t), u(t)\right) \tag{1}$$

where $z \in \mathbb{R}^n$ is the time dependent state vector, $u \in \mathbb{R}^p$ is a time dependent input vector, and t is the time variable. For structural dynamic systems the state variable z is the vector valued function of time $z = \left[x^{\mathrm{T}}\ \dot{x}^{\mathrm{T}}\right]^{\mathrm{T}}$ composed of the N displacement degrees of freedom (DOF) $x \in \mathbb{R}^N$ and the N time derivatives of the displacement DOF, $\dot{x}$, where n=2*N. The superscript 'T' denotes the matrix transpose operator. It is assumed that f is a C^1 (at least one-time continuously differentiable) nonlinear function defined on an open subset of $\mathbb{R}^n$ that contains all the possible positions and velocities of the system of interest. For a specific input, the vector field f generates the flow $Z_t \in \mathbb{R}^n$ that contains families of solution curves of the differential equation [43]. A single solution curve is defined by its initial state vector z_0 and input vector u_0 and by tracing the flow $Z_t(z_0)$ for a finite time.

This work considers systems with harmonic forcing so $\overline{u}(t+T) = \overline{u}(t)$ and hence $\dot{z} = f\left(z, T\right)$, where the dependence of the system on the fundamental period T is explicitly shown. Under these conditions and when the system reaches steady state, it is assumed that the flow contains at least one periodic orbit γ with period T, and $\overline{z}(t+T) = \overline{z}(t)$ for any state $\overline{z} \in \gamma$. (From here forward, the overbar will be dropped from the state vectors when talking about states from a periodic orbit in order to simplify the notation.) Depending on the configuration of the system and its parameters, including the forcing frequency and amplitude, the flow may contain multiple periodic orbits [43, 44]. Tracking the periodic orbits in a nonlinear system can be difficult because a small change in the parameters of the system, such as the forcing frequency, may drastically change the dynamics of the flow. For example, a stiffening system has a frequency response peak that bends to higher frequencies, and

the response can jump from a high amplitude response to a very low amplitude response as the frequency is increased beyond the critical value. In order to characterize all of the periodic orbits that exist in the flow of the differential equation, one must calculate each pairing of initial state vector and period (z_0, T) of the orbits.

This work presents a continuation method that is used to calculate many of the periodic orbits of the differential equation, thereby producing a frequency response function. The general procedure is outlined below and shows the different steps of the algorithm.

1. Provide a starting guess: $(z_{0,(0)},T_{(0)})$
   - The method begins after the user supplies $(z_{0,(0),}\ T_{(0)})$ where the subscript zero in parentheses designates that these conditions are the starting initial conditions.
2. Calculate a starting solution: $(z_{0,(1)},T_{(1)})$
   - The proposed continuation method must be started from an actual periodic orbit of the system. To calculate this first solution, a Newton-Raphson correction method (NRCM 1), which accounts for changes in both the state vector Δz_0 and the period ΔT, can be employed to calculated the first periodic orbit solution $(z_{0,(1)},T_{(1)})$.
3. Initiate the predictor-corrector procedure to calculate a branch of solutions: $(z_{0,(j)},T_{(j)})$, j=1,2,3,4,…
   a. Prediction Step: $(z_{0,pr,(j+1)},T_{pr(j+1)})$
      - The current solution is used to calculate a prediction $(z_{0,pr,(j+1)},\ T_{pr(j+1)})$ for the initial conditions of the next periodic solution. The prediction is then corrected to find a true solution near the predicted one.

   b. Correction Step: $(z_{0,(j+1)}^{(k)},T_{(j+1)}^{(k)})$, k =1,2,3,…
      - The prediction step is used as the initial guess, $(z_{0,(j+1)}^{(0)},T_{(j+1)}^{(0)})$, for the second Newton-Raphson procedure. The second Newton-Raphson correction method (NRCM 2) includes all the equations from NRCM 1, but it has an additional equation that constrains the corrections to be orthogonal to the prediction. NRCM 2 is used to calculate corrections to the initial conditions, $(z_{0,(j+1)}^{(k)},T_{(j+1)}^{(k)})$, until the $(j+1)^{th}$ periodic solution is obtained.
      - If a solution is obtained: After each $(j+1)^{th}$ solution is calculated, Step 3 is repeated.
      - If a solution is not obtained: If the convergence criteria are not met within some pre-set number of iterations:
        1. The procedure calculates a new prediction, $(z_{0,pr,(j+1)},T_{pr(j+1)})$, using a smaller step and the correction portion of Step 3 is restarted.
        2. The procedure switches to a third form of the Newton-Raphson correction method (NRCM 3). This form accounts for changes in the state vector Δz_0 only, so that the period is held fixed (i.e. ΔT=0), and there are no geometric constraints placed on the corrections. The prediction initial condition is used for an initial guess, and the NRCM 3 is used to calculate the periodic solution. When the solution is calculated, Step 3 above is repeated.

The details of this procedure will be provided below, but first the general Newton-Raphson correction method is derived. Some parts follow the derivation from [24], but there are several differences that arise due to the forcing, which causes the function f in Eq. (1) to depend explicitly on time, t, and on the period, T, of the forcing frequency.

2.1 Shooting Function

The proposed method is an iterative process that seeks to find the periodic solutions of a system for different forcing frequencies. The *shooting function* is created to quantify whether a certain set of initial conditions, (z_0, T) produce a periodic response. First, the forcing frequency is set to $\Omega=2\pi/T$ and Eq. (1) is integrated over the interval (0, T) from an initial state vector z_0. Then, the shooting function $H \in \mathbb{R}^n$ is defined as

$$H\left(z_0,t,T\right) \equiv z_T(z_0,t,T) - z_0 \tag{2}$$

where $z_T=z(z_0,\ t=T,T)$ is the state vector found by integrating with initial condition z_0 until $t=T$. This equation represents a two-point boundary value problem for the periodic orbit of the system where the forcing has zero phase at t=0 and $t=T$. Eq. (2) will be satisfied when $H\left(z_0,T\right)=\left\{0\right\}$. In practical numerical computation, the shooting function will be satisfied when $H(z_0,T) \approx \left\{0\right\}$ for some chosen convergence criterion. In this work, the convergence criterion defined in [24] is used

$$\frac{\left\|H\left(z_0,T\right)\right\|}{\left\|z_0\right\|}=\frac{\left\|z_T-z_0\right\|}{\left\|z_0\right\|}<\varepsilon \tag{3}$$

where ε=1e-6 is the convergence value. Each time the equations of motion are integrated over the assumed period, the shooting function is subsequently calculated and the convergence is evaluated.

2.2 Newton-Raphson Correction Methods

When the given calculation of the shooting function does not satisfy the convergence criterion, a Newton-Raphson [25] method is used to calculate updates Δz_0 and ΔT to the initial conditions. Following the approach used in [24], the shooting function can be expanded in a Taylor series about $\left(z_0+\Delta z_0, T\ +\Delta T\ \right)$,

$$H\left(z_0,t=T,T\right)+\left.\frac{\partial H}{\partial z_0}\right|_{\left(z_0,T\right)}\Delta z_0+\left.\frac{\partial H}{\partial T}\right|_{\left(z_0,T\right)}\Delta T=\left\{0\right\}, \tag{4}$$

where only the linear terms have been retained. The partial derivatives in the Taylor expansion must be carefully calculated. The first partial derivative, $\left[\partial H/\partial z_0\right]\in\mathbb{R}^{nxn}$, has the same form as in [24], and can be expanded as

$$\left.\frac{\partial H}{\partial z_0}\right|_{\left(z_0,T\right)}=\left.\frac{\partial z(z_0,t,T)}{\partial z_0}\right|_{t=T}-\left[I\right] \tag{5}$$

where [*I*] is the *n*x*n* identity matrix. The time varying Jacobian matrix $\left[\partial z/\partial z_0\right]\in\mathbb{R}^{nxn}$, which is the variation of the state vector at time *t* due to a small change in the initial conditions, can be calculated using one of two methods described in detail in [24]. The first method, which uses a finite differences approach, can be used even when the equations of motion are not available in closed form, but it is more computationally expensive so it is not used in this work. The second approach is to form the following system of time varying differential equations by differentiating Eq. (1) with respect to z_0, switching the order of differentiation on the left hand side, and applying the chain rule on the right hand side.

$$\frac{d}{dt}\left(\frac{\partial z(z_0,t,T)}{\partial z_0}\right)=\left[\left.\frac{\partial f(z,t,T)}{\partial z}\right|_{z=z(t)}\right]\left[\frac{\partial z(z_0,t,T)}{\partial z_0}\right] \tag{6}$$

In this equation, the Jacobian matrix $\left[\partial f/\partial z\right]\in\mathbb{R}^{nxn}$ is simply the linearization of *f* about the state *z*(*t*) for each time instant *t* in the interval (0, *T*). Since, the state response was calculated on the interval (0, *T*) in order to evaluate the shooting function, it can be easily stored in order to integrate the system of Eq. (6) from initial conditions $\left[\partial z(z_0,t=0,T)/\partial z_0\right]=\left[I\right]$. The solution matrix $\left[\partial z/\partial z_0\right]$ can then be evaluated at *t* = *T* and used to calculate $\left[\partial H/\partial z_0\right]$.

The vector $\left\{\partial H/\partial T\right\}\in\mathbb{R}^n$ in Eq. (4) differs from the result presented in [24], since the function *f* depends explicitly on *t* and *T*. This partial derivative can be expanded using the chain rule as

$$\frac{\partial H}{\partial T}=\left.\frac{\partial H}{\partial t}\right|_{t=T}+\left.\frac{\partial H}{\partial T}\right|_{t=T} \tag{7}$$

where the first term represents the change in the shooting function due to a change in the instant that is taken to be the end of the period and can be calculated from Eq. (1) as in [24].

$$\left.\frac{\partial H}{\partial t}\right|_{t=T}=f(z_T,t=T,T) \tag{8}$$

The second term in Eq. (7) was not present in [24], but arises here due to the forcing since $f(z,t,T)$ has explicit dependence on the period of the forcing, T. The term represents the change in the shooting function due to a change in the period of the input.

$$\left.\frac{\partial H}{\partial T}\right|_{t=T} = \left.\frac{\partial z(z_0,t,T)}{\partial T}\right|_{t=T} \tag{9}$$

Note that the second term of the shooting function does not appear in either of these expressions because $\{\partial z_0/\partial T\} = \{0\}$. Using the same approach that was used to derive Eq. (6), one can derive the following system of time varying differential equations that can be solved to calculate $\{\partial z/\partial T\}$.

$$\frac{d}{dt}\left(\frac{\partial z(z_0,t,T)}{\partial T}\right) = \left[\left.\frac{\partial f(z,t,T)}{\partial z}\right|_{z=z(t)}\right]\left\{\frac{\partial z(z_0,t,T)}{\partial T}\right\} + \frac{\partial f}{\partial T} \tag{10}$$

The term $\{\partial f/\partial T\} \in \mathbb{R}^n$ has arisen because $f(z,t,T)$ and $z(z_0,t,T)$ both have explicit dependence on the period of the forcing, T. Hence, this second set of differential equations must be integrated from initial conditions $\{\partial z(z_0,t=T,T)/\partial T\} = f(z_T,t=T,T)$ over the interval (0,T) in order to compute $\{\partial z(z_0,t,T)/\partial T\}$.

After calculating partial derivatives in Eq. (4), an algebraic system of equations can be formed to solve for an update (Δz_0, ΔT) to the initial conditions. These partial derivatives are used in slightly different ways at different steps in the continuation algorithm, as explained below.

2.3 Continuation Procedure

2.3.1 Provide a starting guess: $(z_{0,(0)},T_{(0)})$

In order to start the continuation procedure, the user must supply a starting guess. A good starting point guess $(z_{0,(0)},T_{(0)})$ consists of a low frequency (i.e. a long period) solution for the underlying linear system (i.e. for $T_{(0)}$ the underlying linear system can be solved for the periodic conditions $z_{0,(0)}$). This is often called a Homotopy approach [18, 25].

2.3.2 Calculate a starting solution: $(z_{0,(1)},T_{(1)})$

The starting guess is used to calculate a set of initial conditions (z_0, T) that lead to a shooting function, $H(z_0,T)$, that satisfies convergence. To calculate the starting solution, the system is integrated from the starting guess, the shooting function is calculated, and the convergence is evaluated. If the initial guess does not satisfy convergence, then the partial derivatives are calculated and the following system is formed to calculate corrections to both the state vector Δz_0 and the period ΔT. This system is the NRCM 1 mentioned above.

$$\begin{bmatrix} \left.\frac{\partial H}{\partial z_0}\right|_{(z_0,T)} & \left.\frac{\partial H}{\partial T}\right|_{(z_0,T)} \end{bmatrix}\begin{Bmatrix} \Delta z_0 \\ \Delta T \end{Bmatrix} = \begin{Bmatrix} -H(z_0,t=T,T) \\ 0 \end{Bmatrix} \tag{11}$$

The right hand side vector contains the vector value of the shooting equation. The new initial conditions are ($z_{0,(1)}= z_{0,(1)}+\Delta z_0$, $T_{(1)}= T_{(0)}+ \Delta T$). Since the period has been updated the harmonic forcing frequency must also be updated in the equations of motion (i.e. $\Omega_{update}=2\pi/(T_{(1)})$ such that $u=u(\Omega_{update}t)$. Then, these new conditions are used to integrate the equations of motion and check the shooting function for convergence. One then repeats this two stage process until the desired convergence is achieved at which point the first periodic orbit solution $(z_{0,(1)},T_{(1)})$ has been calculated. The Newton-Raphson corrector method is a local technique, so the starting guess, $(z_{0,(0)},T_{(0)})$, must be close to the actual solution or the correction scheme will diverge. The first periodic orbit solution and the Jacobian matrices that were used to produce it can be used to initiate the next step.

2.3.3 Initiate the predictor-corrector procedure to calculate a branch of solutions: $(z_{0,(j)},T_{(j)})$, j=1,2,3,4,…

In order to calculate an entire branch of solutions, an adaptive *pseudo arc-length* continuation [28] method is employed that uses a prediction step which is followed by a correction step. Predictor-corrector methods can follow complex solution braches because the prediction step follows the direction in which the branch of solutions actually evolves. The prediction step, which is calculated using information from the current periodic solution, is used to calculate new initial conditions for the next periodic orbit. The prediction step can be further adapted to evaluate the convergence of the previous correction steps and adjust the step size accordingly. After the prediction step, the shooting method is employed, but now with a new Newton-Raphson correction method that varies the state vector and the forcing frequency in a constrained direction.

2.3.3.1 Prediction Step: $(z_{0,pr,(j+1)},T_{pr,(j+1)})$

The basic process is to use the previous periodic orbit solution, which is denoted as the j^{th} solution, to calculate a tangent predictor step for the $(j+1)^{th}$ periodic orbit conditions, including a prediction for the initial state vector and the forcing period. The prediction $\{P\} \in \mathbb{R}^{n+1}$, which has components $\{P_z\} \in \mathbb{R}^n$ and $P_T \in \mathbb{R}$ corresponding to the states and period respectively, is the tangent vector to the solution branch and can be calculated with the following system of equations.

$$\left[\left.\frac{\partial H}{\partial z_0}\right|_{\left(z_{0,(j)},T_{(j)}\right)} \quad \left.\frac{\partial H}{\partial T}\right|_{\left(z_{0,(j)},T_{(j)}\right)}\right]\left\{P_{(j)}\right\} = \begin{Bmatrix}\{0\}\\ 0\end{Bmatrix} \tag{12}$$

$$\left\{P_{(j)}\right\} = \left[P_{z,(j)}^{\mathrm{T}} \; P_{T,(j)}\right]^{\mathrm{T}}$$

The components of the left hand side matrix come from the Taylor series expansion of the shooting function, and were previously defined. They characterize the vector space that is normal to the periodic solution curve, and once they are found, the desired tangent vector $\{P\}$ in Eq. (12) is simply the vector that is in the null space of the matrix on the left in Eq. (12). Once the tangent vector $\{P\}$ has been calculated it can be normalized to unit length, and the predictions for the next periodic solution can be calculated with

$$z_{0,pr,(j+1)} = z_{0(j)} + s_{(j)}P_{z,(j)} \tag{13}$$

$$T_{pr,(j+1)} = T_{(j)} + s_{(j)}P_{T,(j)} \tag{14}$$

$$\Omega_{pr,(j+1)} = 2\pi/T_{pr,(j+1)} \tag{15}$$

where $z_{0,pr,(j+1)}$ and $T_{pr,(j+1)}$ are the prediction initial conditions for the $(j+1)^{th}$ solution and $s_{(j)}$ is the j^{th} step size. One must be sure to again update the differential equations so that the external forcing reflects the change in frequency (i.e. $u=u(\Omega_{pr,(j+1)}t)$).

The step size is critical to the success and efficiency of the computation. One can fix the step size to a very small value and ensure that very small increments are made between successive solutions, but this can be impractical because computation times may be long. A better approach is to provide an automated step size control algorithm. In this work, the step size control algorithm from [24] is employed. The first step size is provided by the user, while all subsequent step sizes are determined by the following equation

$$s(j) = sign\left(s_{(j-1)}\left\{P_{(j)}\right\}^{\mathrm{T}}\left\{P_{(j-1)}\right\}\right)\left(\frac{K^*}{K_{(j-1)}}\right)\left|s_{(j-1)}\right| \tag{16}$$

where $K_{(j-1)}$ is the integer number of iterates that were required to update the previous shooting function solution and K^* is an optimal number of shooting iterates which is supplied by the user. The signum function $sign(\bullet)$, ensures that the step used to calculate the predictions follows the solution curve in the same direction. Furthermore, it is helpful to place maximum and minimum bounds on the step size. When the step size is increased beyond these bounds, it can be automatically reduced below the maximum or increased above the minimum.

2.3.3.2 Correction Step: $(z_{0,(j+1)}^{(k)}, T_{(j+1)}^{(k)})$, k =1,2,3,…

As discussed in [24], the Newton-Raphson updates to the shooting functions can be made more efficient by forcing the corrections to be orthogonal to the tangent predictor vector. Therefore, at this point in the algorithm the correction steps are calculated with the following algebraic system, which is the NRCM 2 mentioned previously,

$$\begin{bmatrix} \left.\dfrac{\partial H}{\partial z_0}\right|_{\left(z_{0,(j+1)}^{(k)}, T_{(j+1)}^{(k)}\right)} & \left.\dfrac{\partial H}{\partial T}\right|_{\left(z_{0,(j+1)}^{(k)}, T_{(j+1)}^{(k)}\right)} \\ \left\{P_{z,(j)}\right\}^{\mathrm{T}} & P_{T,(j)} \end{bmatrix} \begin{Bmatrix} \Delta z_{0,(j+1)}^{(k)} \\ \Delta T_{(j+1)}^{(k)} \end{Bmatrix} = \begin{Bmatrix} -H\left(z_{0,(j+1)}^{(k)}, T_{(j+1)}^{(k)}\right) \\ 0 \\ 0 \end{Bmatrix} \tag{17}$$

where all the components have been previously defined. The solution to this equation provides the k^{th} corrections $\Delta z_{0,(j+1)}^{(k)}$ and $\Delta T_{(j+1)}^{(k)}$ to the guess for the $(j+1)^{th}$ solution. The algorithm then alternates between a shooting function calculation $H(z_{0,(j+1)}^{(k)}, T_{(j+1)}^{(k)}) \approx \{0\}$ and a correction step calculation $z_{0,(j+1)}^{(k+1)} = z_{0,(j+1)}^{(k)} + \Delta z_{0,(j+1)}^{(k)}$ and $T_{(j+1)}^{(k+1)} = T_{(j+1)}^{(k)} + \Delta T_{(j+1)}^{(k)}$, where $k = 0,..,K_{(j+1)}$. The integer $K_{(j+1)}$ is the number of correction iterations required to converge on the solution and k=0 corresponds to the predictions $z_{0,(j+1)}^{(0)} = z_{0,pr,(j+1)}$, $T_{(j+1)}^{(0)} = T_{pr,(j+1)}$. When one of the correction steps leads to a shooting function that converges, then the periodic orbit solution is stored and a new prediction is calculated as the algorithm advances to the $(j+2)^{th}$ step.

In some cases the correction steps may diverge (i.e. the norm of consecutive shooting function values may increase instead of decreasing to zero), or they may converge very slowly. In order to account for these issues, the shooting function values can be tracked to ensure that the norm of consecutive shooting functions are decreasing and the number of correction steps can be bounded with K_{max}. In this work, when either of these constraints is not met, the following two procedures are initiated in order to try to find a solution. The default procedure is to calculate a new prediction using a smaller step size. In particular, the step size is divide by two, $s(j)=s(j)/2$, Eqs. (13-15) are recalculated, and the correction step procedure is followed again. Usually, for small enough step sizes, the predicted initial guess is close to the previous periodic solution, and the algorithm is likely to converge on the new solution. However, the authors have found cases where this does not always lead to convergence. Therefore, a minimum step size is defined that is on the order of the convergence value. When the minimum step size is surpassed, the algorithm tries a second alternate procedure that uses the current prediction step initial conditions, $(z_{0,pr,(j+1)}, T_{pr,(j+1)})$, which were just recalculated with the minimum step size. First, the predictions are used as the initial conditions for the next solution (i.e. $z_{0,(j+1)}^{(0)} = z_{0,pr,(j+1)}$, $T_{(j+1)} = T_{pr,(j+1)}$), but the period is fixed such that there will be no correction calculated (i.e. $\Delta T_{(j+1)}^{(k)}$ =0). Then, a solution is calculated with the following NRCM 3 system

$$\left[\left.\frac{\partial H}{\partial z_0}\right|_{\left(z_{0,(j+1)}^{(k)}, T_{(j+1)}\right)}\right] \Delta z_{0,(j+1)}^{(k)} = -H\left(z_{0,(j+1)}^{(k)}, T_{(j+1)}\right). \tag{18}$$

where corrections are calculated only for the state vector $\Delta z_{0,(j+1)}^{(k)}$. Once convergence is obtained the solution is stored and the predictor-corrector method returns to the prediction step above.

2.3.4 Discussion

The proposed algorithm is used to calculate an entire branch of solutions. The starting and stopping frequencies must be input by the user. Additionally, the step size must be very carefully monitored and controlled (by maximum and minimum step size bounds and by setting the appropriate values of K^*). The algorithm typically converges and produces good results, but sometimes the algorithm parameters do still need to be manually adjusted during the calculations to provide convergence or at least efficient computation.

2.4 Computational Efficiency

Nonlinear systems are inherently sensitive to changes in the harmonic forcing, so other manual control techniques may also be required to efficiently calculate frequency response functions. Harmonically forced nonlinear systems exhibit responses similar to linear systems with resonance peaks near linear natural frequencies and low response bands between away from resonance peaks. Therefore, the turning points are likely to be located near the linear natural frequencies. Away from those frequencies, where the response is low and in general very flat, it may be more efficient to apply *sequential continuatio*n, where the frequency band of interest is divided into a number of evenly spaced frequency values and a solution for each is sought sequentially. When this is done, NRCM 3 can be used as a method to calculate the periodic solutions at each frequency value in the interval. Because there are fewer calculations involved and hence less computation time required, the sequential method may be more efficient for the regions away from resonance, but it fails near resonance where the response amplitude can change dramatically with a small change in frequency. A very efficient algorithm is one that seamlessly switches between different types of continuation depending on which type is currently the most efficient. One can quantify the efficiency of the method being used by assessing the number of iterations it takes before a periodic solution is achieved (i.e. if $K_{(j)}$ is consistently larger than K^*, one might switch methods). These types of constraints were not included for this work because the solution branches for the systems considered were calculated efficiently with the proposed method, but such constraints can easily be added to the procedure.

2.5 Stability of Periodic Orbits

Using the proposed method, the stability of a periodic orbit can be calculated whenever convergence of a periodic solution is achieved (this was also discussed in [24]). The matrix $\left[\partial z(z_0, t=T, T)/\partial z_0\right]$ in Eq. (5) from the final Newton-Raphson calculation ($k=K_{(j+1)}$) is the Monodromy matrix [45] of the periodic orbit. (Recall that it was formed from a linearization of the system about its periodic orbit and was calculated at $t = T$.) The stability of this periodic orbit can be determined from the eigenvalues of this matrix. If the eigenvalues of the Monodromy matrix are inside (outside) the unit circle, then the orbit is stable (unstable). So the stability of periodic solution is conveniently found without additional calculations when using this method.

3. Application to a Duffing Oscillator

Figure 1 illustrates a single degree of freedom Duffing oscillator, which will be used to illustrate the proposed algorithms. The system has a discrete mass m with displacement degree of freedom x. The system mass is connected to a dashpot with damping coefficient c and to a linear spring with spring stiffness k and a nonlinear spring with spring constant k_3. External forcing is applied with F_d.

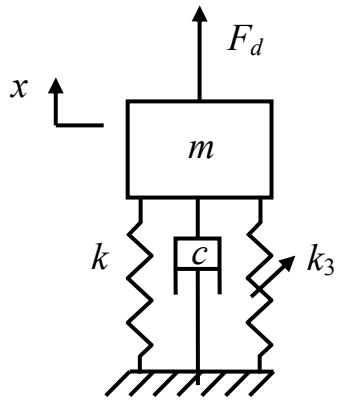

Fig. 1 Single degree of freedom oscillator with a nonlinear spring.

The nonlinear spring provides a quadratic nonlinear spring stiffness k_3x^2, so the equation of motion for the Duffing oscillator is given by the following,

$$m\ddot{x} + c\dot{x} + kx + k_3x^3 = F_d \tag{19}$$

which can be written as follows in the state space after first dividing through the entire equation by m and defining the nondimensional parameters $2\zeta\omega = c/m$, $\omega^2 = k/m$, $\omega_3^2 = k_3/m$, and $F = F_d/m$ where ζ is the coefficient of critical damping.

$$\begin{Bmatrix} \dot{x} \\ \ddot{x} \end{Bmatrix} = \begin{Bmatrix} \dot{x} \\ -2\zeta\omega\dot{x} - \omega^2 x - \omega_3^2 x^3 + F \end{Bmatrix} \tag{20}$$

The parameters used in this study are: ζ=0.01, ω=1, and ω_3=0.5. The system is driven with the following harmonic forcing function

$$F(t) = A\sin(\Omega t) \tag{21}$$

where A is the forcing amplitude and Ω is the circular driving frequency. The proposed continuation algorithm will be used to calculate an entire branch of state solutions for a range of forcing frequencies between Ω=0.1 and 10 rad/s and for three different forcing amplitudes: A=0.01, 0.1, and 1. The starting guess for the algorithm was calculated from the underlying linear system that was forced at Ω=0.1 rad/s. The algorithm was then allowed to run in an automated fashion until the solutions were found for a forcing frequency of at least of 10 rad/s. Since the linear natural frequency of this system is ω=1 rad/s, the largest responses are expected to occur within this frequency band.

Figure 2 shows the periodic solution curves, which are plotted versus forcing frequency, for forcing amplitude A=0.01. The forcing frequencies in the all of the following plots are normalized by dividing by the linear natural frequency ω=1 rad/s so that the abscissa values are reported as dimensionless values of Ω/ω. The state displacement initial condition is plotted in (a), and the state velocity initial condition is plotted in (b). When a displacement and velocity pair is chosen for a specific frequency, these initial conditions and forcing frequency can be integrated for time T=2π/Ω to provide the full trajectory of the corresponding periodic orbit. In the figure, the solutions to stable periodic orbits are shown with solid lines (FCont Stable) and the unstable periodic orbit solutions are shown with dashed lines (FCont Unstable). The stable periodic orbit solutions were verified by using extended time integration (Ext Int), shown with open circles. The first extended integration solution was also used as the initial guess for the continuation algorithm. For all of the subsequent solutions with extended integration, the solution at the previous forcing frequency was used as an initial condition and the system was integrated until it reached a steady state periodic orbit. The solution branch calculated with the continuation algorithm agrees very well with the solutions calculated with extended integration. The distinct resonance peak in the displacement curve is similar to that of a linear, single degree of freedom frequency response function, but it appears to bend slightly to the right. Moreover, the solutions on the lower frequency arm of the peak are stable while some of the solutions on the higher frequency arm of the peak are unstable. When the displacement peaks near Ω/ω=1, the velocity magnitude becomes large and negative, but as the frequency increases the velocity goes through a zero and then sharply becomes large and positive. The inset axes in (b) shows a detail view of the sharp peak in the velocity curve. It reveals the unstable solutions in the velocity curve, which form a loop turning point. For higher frequencies, the displacement and velocity decrease to very small positive values.

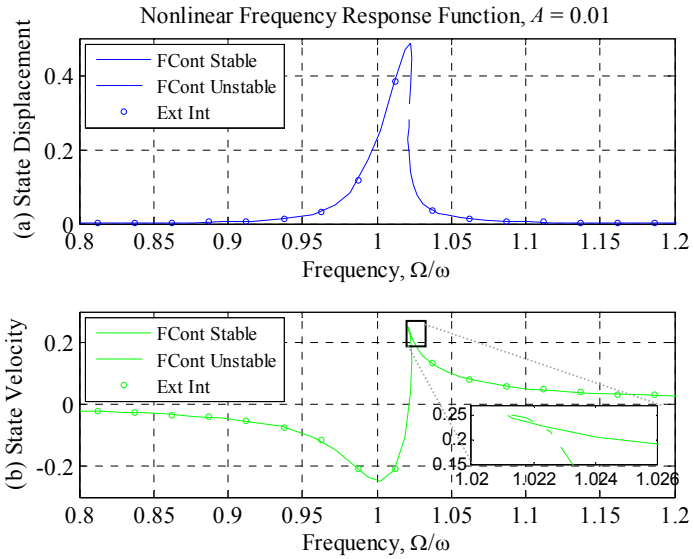

Fig. 2 Initial conditions that result in periodic responses for A=0.01 plotted versus dimensionless forcing frequency

When the forcing amplitude is A=0.01, the response of the system is nearly linear. The displacement values in the figure are very characteristic of a linear frequency response function, and the peak in the displacement bends only slightly towards higher frequencies due to hardening [18]. However, as evinced in the figure, there is a small portion of the displacement solution branch that is unstable and where multiple responses are possible for a single value of forcing frequency.

The same procedure was followed after increasing the forcing amplitude to A=0.1. The periodic solutions for displacement and velocity initial conditions, 3(a) and 3(b), respectively, are plotted in Figure 3. Several periodic solutions that were calculated with extended integration are also shown, marked by open circles, and similar to the first case the agreement is very good. There is a sharp peak in the displacement versus frequency curve, which starts to increase in amplitude near Ω/ω=1. The maximum amplitude of this peak occurs near Ω/ω=1.65. Unlike a linear response curve, this peak bends strongly to higher frequencies. The lower frequency arm of the peak contains stable solutions, while the higher frequency arm of the peak has unstable periodic solutions until the displacement amplitude reaches a low value again. The velocity curve 3(b) has a large loop in it. The lower half of the loop contains the stable solutions that correspond to the lower frequency arm of the displacement peak. When the displacement curve reaches its maximum value, the velocity goes through zero and then enters the upper half of the loop, which contains the unstable solutions. There is a significant band between Ω/ω= 1.1 and 1.65 where multiple periodic solutions exist for single forcing frequencies, so the actual response observed depends on the initial conditions and the system's response might jump between those solutions if perturbed.

The inset in 3(a) provides a detailed view of the tip of the displacement versus frequency curve. In this expanded view the stable orbits that were found with continuation are marked with dots and the unstable ones with open squares. Near the tip the solutions that were found are very closely spaced, revealing that the continuation algorithm required small predictor steps in this region. The turning point in the displacement peak is very sharp, yet the continuation algorithm calculates the turn accurately by automatically reducing the step size between successive periodic solutions.

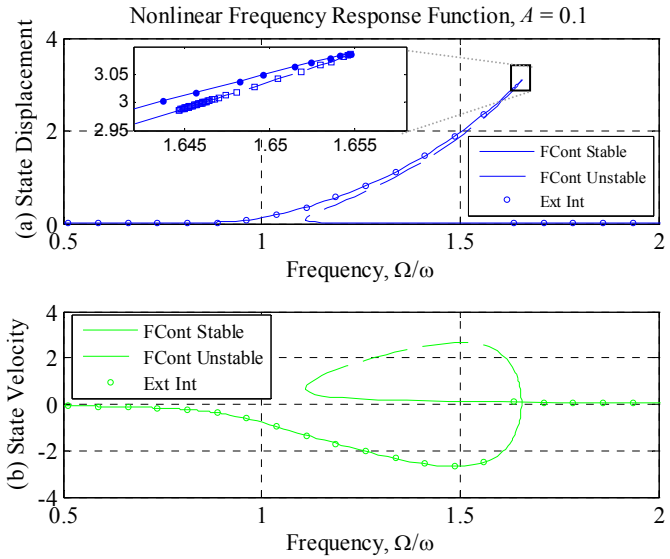

Fig. 3 Initial conditions that result in periodic responses for A=0.1 plotted versus dimensionless forcing frequency

In the final case, a forcing with amplitude of A=1 is applied to the system and the results are shown in Figure 4, in the same format as the previous cases. Solutions were calculated with extended integration and are shown again with the open circles, although for frequencies above Ω/ω= 1.35 only every tenth extended integration solution is plotted for clarity. The displacement solution branch in 4(a) has a large sharp peak that bends significantly to higher frequencies over the range of Ω/ω=1.5 to 4.7. Here, the displacement solutions are plotted with a logarithmic scale for the ordinate because there lower frequency and higher frequency arms of the large peak are very close to each other. The shape of the bent peak on a linear scale has a very similar form to that in Figure 3(a). The higher frequency arm of the bent peak is plotted with a dashed line. The velocity solution branch has a very similar shape to the velocity periodic solution curve of the previous forcing case. The main difference is that the large loop reaches larger negative and positive values for the lower solid line and upper dashed line, respectively. At low frequencies, the displacement shows several sharp peaks that have smaller magnitude than the dominant peak in the curve. Figure 5 shows a detailed view of the displacement and velocity curves for a frequency band of Ω/ω=0.1 to 0.5. The displacement curve peaks near Ω/ω = 0.1, 0.13, 0.16, 0.23, and 0.39, and the peak near 0.39 appears to bend towards higher frequencies. As the displacement peaks near Ω/ω=0.39, the velocity condition curve changes from negative to positive and contains a small loop, which is very similar in shape the velocity initial condition curve of Figure 2(b). All of the periodic orbit solutions calculated with extended integration in Figures 4 and 5 agree very well with the results produced with the continuation algorithm.

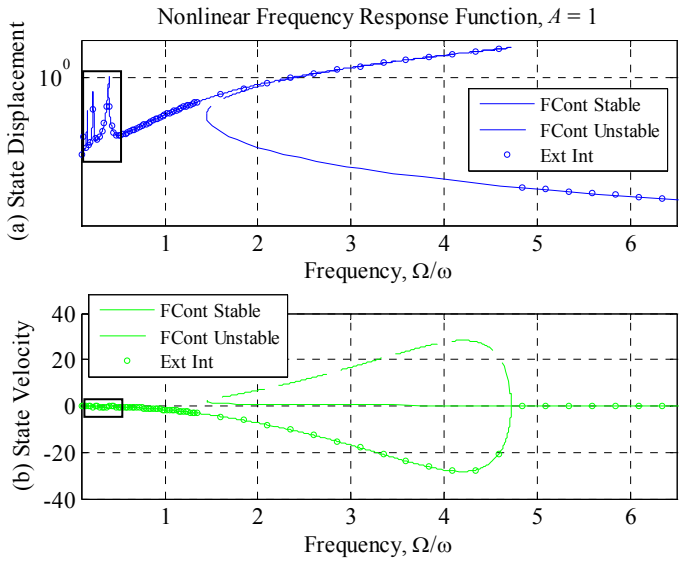

Fig. 4 Initial conditions that result in periodic responses for A=1 plotted versus dimensionless forcing frequency

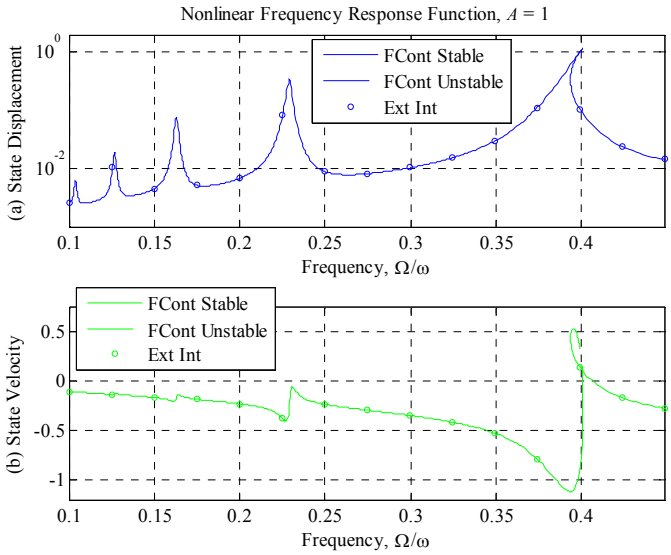

Fig. 5 Expanded view of the region indicated with a box in Figure 4

When the forcing amplitude is A=1, the system exhibits strong nonlinearity. The displacement curve shows a very strong spring hardening effect, so that multiple solutions exist for the frequencies from Ω/ω=1.5 to 4.7. There are three periodic orbits for most of this region. Two of these orbits are stable and correspond to low and high amplitude responses to the same forcing function. The third orbit is unstable and similar to the higher amplitude branch. Because the unstable orbit is close to the stable orbit, it is difficult to calculate either of the periodic orbits along these curves, especially with extended integration. A very small frequency increment had to be used when the extended integration procedure, otherwise the system would tend to settle to the very small amplitude branch. The continuation algorithm does not have this problem, and is able to calculate both the stable and unstable branches in this region with great detail. The numerous superharmonic resonance peaks [18, 19] are another consequence of the strong forcing amplitude. These tend to occur when the drive frequency is a fraction of the linear natural frequency. One can see from Figure 5 that it is very easy to miss the detail of these phenomena when using extended integration unless a very small frequency increment is used. Furthermore, when using other techniques such as harmonic balance, a separate analytical derivation would have to be performed for each of the peaks. Using the forced continuation approach presented here, these peaks are automatically detected and are well resolved.

3.1 Discussion

The periodic solutions that were calculated with continuation were verified using extended integration, but these calculations took approximately an order of magnitude longer to compute. In frequency bands where multiple periodic orbits exist for single forcing frequencies, the extended integration method will seem to settle at random on different parts of the periodic solution curve. Extended integration has to be carefully used with the appropriate initial conditions to remain on a given curve. For example, in Figure 3 extended integration solutions are calculated for many points at frequencies below the resonance, but no solutions were found on the low amplitude branch between Ω/ω = 1.2 and 1.65 because the initial conditions used for each extended integration calculation were from the previous periodic orbit solution, and the procedure was started at low frequency. This could have been remedied by starting at high frequency, but in any event the extended integration method could not be used to calculate the unstable periodic orbits, because the system will not naturally settle on an unstable orbit.

The accuracy of the forced continuation solutions can also be verified by calculating the maximum magnitude of each periodic orbit for the different forcing frequencies and amplitudes. When these values are plotted versus the forcing frequency, the result is the traditional frequency response curve in terms of the magnitude of the response. Furthermore, the method in [24] can be used to calculate the unforced periodic solutions of the system, which should provide the backbone curve of the nonlinear frequency response functions. Figure 6 shows the results of these calculations. The nonlinear frequency response curves are plotted for A= 0.01, 0.1, and 1 with a blue, green, and red line, respectively. The unstable solutions are plotted with a dashed line. The periodic solutions of the conservative system (i.e. unforced and undamped) are plotted with the black line.

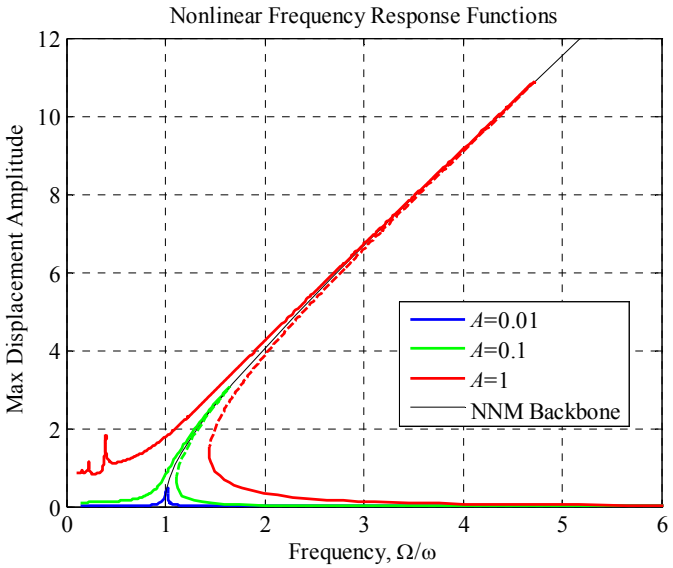

Fig. 6 Conservative System Backbone Curve and Nonlinear Frequency Response Functions for all the Forcing Amplitudes

The forced solutions in the figure track the backbone curve very accurately and the peak of each forced curve crosses the backbone curve. The figure also shows that the frequency response functions do not scale with the magnitude of the forcing, which increases by powers of ten; this is a distinct property of nonlinear systems.

Stability tracking is very convenient with the forced continuation algorithm. Since the Monodromy matrix is calculated as part of the shooting procedure, it can always be used to calculate and store the eigenvalues. These eigenvalues define the stability for each periodic orbit, so one can track the paths of the eigenvalues and quantify the amount of stability or instability each periodic orbit as it is forced at a given frequency. Figure 7 shows the turning point that occurs in the displacement curve near $\Omega/\omega=1.65$ for forcing at $A=0.1$. The top plot, 7(a), shows a magnified view of the displacement curve in the region of interest from Figure 3. For 7(b), the continuous time eigenvalues were calculated by taking the natural logarithm of the eigenvalues from the Monodromy matrix and dividing by the corresponding period. Then, the real part of the continuous time eigenvalue is plotted for the region of interest. In continuous time, stable eigenvalues have negative real parts, and the curve in 7(b) clearly shows that the eigenvalues on the stable curve have essentially constant damping until they quickly jump from stable to unstable as the turning point is crossed.

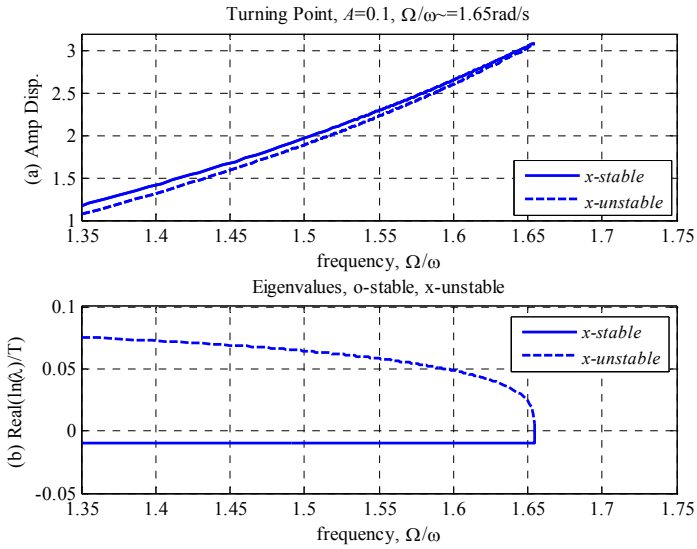

Fig. 7 Turning point near $\Omega/\omega=1.65$ for $A=0.1$ and eigenvalue stability

4. Application to a Nonlinear Beam

The proposed continuation technique is formulated so that it can be easily extended to higher order systems. The second system considered for this work is a cantilever beam with a cubic spring attached to the tip and is shown schematically in Figure 8. The coordinate, x, describes the location along the axis of the beam, y describes the transverse deflection at a given position x, and F_d describes the harmonic external forcing function applied to the beam. The beam is assumed to have uniform parameters: densityρ, elastic modulus E, cross sectional area A_b, transverse moment of inertia I, and length L.

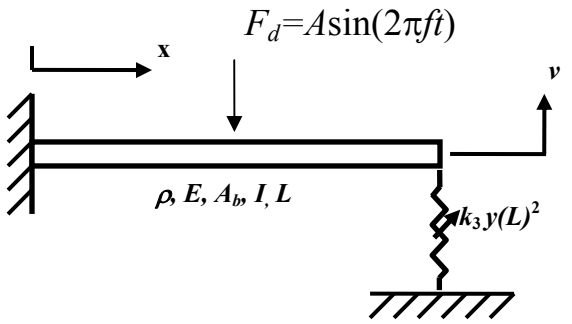

Fig. 8 Cantilever beam with a nonlinear spring attached to the tip.

This system can be achieved in experiment [46, 47], so a model of the beam can be useful to study the periodic responses of the experimental system under different harmonic forcing parameters. A Ritz-Galerkin approach was used to create a two degree of freedom model for the beam where the degrees of freedom are located at the beam's center and tip. In order to reproduce response properties on the order of the responses from the experimental system in Sracic, 2011 #192}, the following parameters were used in for the model: ρ=2700 kg/m^3, E=68e9 N/m^2, A_b=3.23e-4 m^2, I = 4.34e-9 m^4, L = 1.016 m. The equations of motion for this model were derived for a uniform, prismatic beam with these parameters and assuming linear-elastic behavior of the beam so that all of the nonlinearity in the system is due to the nonlinear spring. Only the final result is shown here in state space format, but the full details are provided in [46].

$$\begin{Bmatrix}\{\dot{y}\}\\ \{\ddot{y}\}\end{Bmatrix}=\begin{Bmatrix}\{\dot{y}\}\\ [M]^{-1}\left(-[C]\{\dot{y}\}-[K]\{y\}-k_3 y(L)^3\begin{Bmatrix}\psi_{1,2}\\ \psi_{2,2}\end{Bmatrix}+A\sin(\Omega t)\begin{Bmatrix}\psi_{1,1}\\ \psi_{2,1}\end{Bmatrix}\right)\end{Bmatrix}$$

$$[M]=\begin{bmatrix}0.3989 & 0.0746\\ 0.0746 & 0.1246\end{bmatrix}\text{Kg},\quad [K]=10^4\begin{bmatrix}3.1546 & -0.9886\\ -0.9886 & 0.3945\end{bmatrix}\text{N/m} \tag{22}$$

$$[C]=\begin{bmatrix}1.8166 & -0.3535\\ -0.3535 & 0.3079\end{bmatrix}\text{N/(m/s)},\quad [\psi]=\begin{bmatrix}0.9250 & 1.4015\\ 2.7244 & -1.9637\end{bmatrix}$$

The matrix $[\Psi]$ has the numerical values of the mode vectors for specific position coordinates on the beam (i.e. mode one is column one and degree of freedom one is in row one). Using these properties with the Ritz-Galerkin method, the two linear natural frequencies of the system were equal to f_1= 9.97 Hz and f_2=62.51 Hz. In the experiment, a thin strip of spring steel is mounted between the free end of the cantilever and a fixed support and is used to create the geometric nonlinearity [46]. The transverse stiffness contribution of this element is approximated in the model as k_3=1.4764e9 N/m^3.

The continuation algorithm was used to calculate the periodic solutions of the beam in the forcing frequency range from 5-100 Hz and for a forcing amplitude of A=1.0 N and using a convergence criterion of ε=1e-6. The first periodic solution was calculated by using extended integration on the system, which was initially at rest. Figure **9** shows the periodic solution curves that were calculated with the continuation algorithm. Two dominant resonances are present in this bandwidth, and those are separated into the left ((a) and (b)) and right ((c) and (d)) columns of plots. The displacements in **9** (a) are plotted with a logarithmic scale on the ordinate. The format from the plots in the previous section is used, but here there is an additional degree of freedom, so the displacement for the second degree of freedom is plotted in red and the velocity in black in order to distinguish them. The stable and unstable solutions are designated as before with solid and dashed lines, respectively. Extended integration was used to calculate periodic solutions in the frequency range and those are plotted with

the open circles. The displacement solutions of both degrees of freedom form sharp peaks in (a) that bend strongly towards higher frequencies. The solutions for the second degree of freedom are larger in magnitude since it is located at the tip of the cantilever which is very active when the first mode is excited. As the frequency increases, the peaks of both degrees of freedom converge on near the same point. There is a small positive and negative peak in the low amplitude displacement curves near 21 Hz, and the negative peak in the red curve shows as a gap due to the logarithmic scale. The solutions for the velocity of degree of freedom one looks similar in shape to some of those for the Duffing oscillator, but the curve for the second degree of freedom is more complicated, changing sign three times before the turning point is reached.

The displacement solution curves for the second mode have opposite signs, as expected since the points are at the midpoint and tip and this is a second bending mode of a cantilever beam. Both curves in (c) have a peak that bends to higher frequencies. There is only a very small region in the curves of the second mode where the solutions are unstable. The frequencies between 23 and 59 Hz were not shown, because all of the solutions were very flat and at low magnitude in that region.

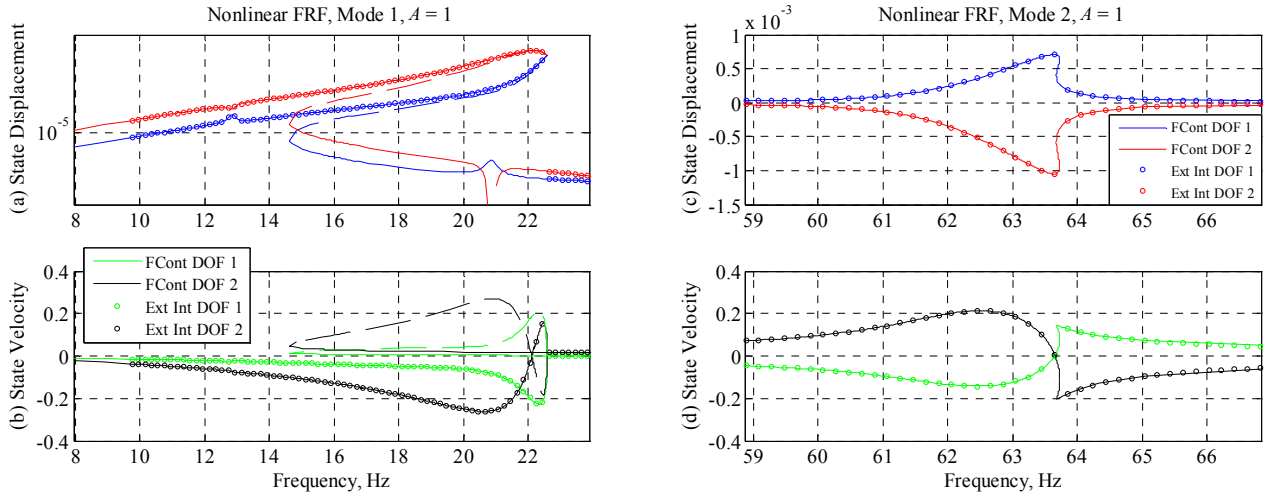

Fig. 9 Initial conditions that result in periodic responses for A=1 plotted versus forcing frequency

The addition of the second degree of freedom brings a lot of new dynamics to the frequency response curves, but many of the same features remain. The peak in the first mode bends across about 12 Hz, so the system response is highly nonlinear for this mode. The region that contains three periodic solutions span about 7 Hz, and in that region, the stable and unstable arms of the peaks are nearly identical in magnitude. The turning point in the peaks occurs near 22.5 Hz, and the curves of the two degrees of freedom seem to deflect towards each other the forcing frequency approaches the turning point. The small peak near 21 Hz in (a) is a superharmonic resonance for the second mode, as evidenced by the fact that this frequency is about a third of the frequency where Mode 2 peaks and the fact that the displacements have opposite signs as in Mode 2. The Mode 1 velocity solution curve for the tip degree of freedom has a second loop in it, and near 22 Hz the three solutions all have very similar values for the velocity of the tip (the location on the curve where the black line crosses three times). Since this curve changes sign three times in the band near 22 Hz, it would be very difficult to obtain an initial guess for extended integration in this region. The second mode is less nonlinear than the first. Except for the sign differences, the curves for modes 1 and 2 resemble the high and low amplitude curves for the Duffing oscillator. The first mode is expected to be more nonlinear than the second because since the effect of discrete springs generally decreases with increasing frequency. The solutions that were calculated with extended integration agree very well with those that were calculated with the continuation technique. As before, the extended integration performed in an upward frequency sweep so some of the solutions were missed with that method.

4.1 Discussion

The continuation algorithm worked well to calculate the periodic solution curves of this two degree of freedom system. The algorithm was generally written for n^{th}-order systems, so the code was the same as that used for the previous cases. The curves included richer dynamics than the single degree of freedom case, and the continuation captured a detailed description of these dynamics. For the higher order system, the calculations naturally took longer than the single degree of freedom case, but the continuation remained at least an order of magnitude faster than extended integration. The calculations can be made faster in regions of very low response (i.e. in the flat response regions between the modes) by allowing the algorithm to

switch into a sequential arc-length continuation, where only the initial conditions for the state vector need to be corrected after the prediction is made. This method switching was applied in this work.

The low frequency superharmonic resonances for the first mode of this beam were not calculated in this work. These phenomena become very complicated for multi-degree-of-freedom systems such as this, especially because the dominant frequency in the periodic orbit may be much higher than the frequency of the forcing. The gradient matrix calculations in the continuation algorithm will be biased towards the dominant terms in the period orbit, and the algorithm has a harder time converging on the periodic orbit solution since it will want to change the frequency to the dominant frequency. These difficulties will be addressed in future work.

5. Conclusions

A pseudo arc-length continuation technique was developed to calculate the periodic solutions for harmonically forced nonlinear systems. The algorithm relies on an initial guess, and then uses a Newton-Raphson updating technique to make corrections to the initial guess in order to converge on an actual periodic orbit solution. This can be done for a single forcing frequency, or over an entire band of forcing frequencies. In order to calculate a curve of solutions as the forcing frequency is varied, a tangent prediction step is calculated from the previous solution and then corrections are made to converge to the next solution. A number of successive solutions can be joined to construct a frequency response curve for the nonlinear system in terms of the steady state amplitudes. The algorithm is applicable to n^{th} order systems, and by construction can follow the path of the solutions around turning points to fully characterize the system's dynamics. Superharmonic, hardening, and softening resonances can all be calculated as long as those phenomena occur in the band over which the frequency is varied. Unstable periodic solutions can also be calculated, and the eigenvalues that determine stability are readily available for all solutions. In this work, the nonlinear frequency response functions were calculated for a single degree of freedom Duffing oscillator at three forcing amplitudes and a two degree of freedom Galerkin representation of a nonlinear beam at one forcing amplitude. The algorithm was able to calculate the detailed frequency response curves of both systems, and the results were verified by integrating the equations of motion for an extended time until they reached steady state. These numerical solutions agreed well with the results calculated with continuation, but the continuation algorithm was at least an order of magnitude faster per periodic orbit solution. Additionally, detailed results were calculated for the superharmonic resonances of the Duffing oscillator, and an eigenvalue migration plot was provided to show the convenience of stability calculations with the proposed method. The nonlinear beam had highly nonlinear frequency response functions since the geometric nonlinearity of the system was so strong, yet its frequency response curves were efficiently calculated over a range of frequencies.

6. References

[1] L. Lin*, et al.*, "Application of AE Techniques for the Detection of Wind Turbine Using Hilbert-Huang Transform," presented at the Prognostics & System Health Management Conference (PHM2010), Macau, China, 2010.

[2] C.-W. Chang-Jian, "Non-Linear Dynamic Analysis of Dual Flexible Rotors Supported by Long Journal Bearings," *Mechanism and Machine Theory,* vol. 45, pp. 844-866, 2010.

[3] G. T. Flowers*, et al.*, "The Application of Floquet Methods in the Analyses of Rotordynamic Systems," *Journal of Sound and Vibration,* vol. 218, pp. 249-259, 1998.

[4] P. Kumar and S. Narayanan, "Nonlinear Stochastic Dynamics, Chaos, and Reliability Analysis for a Single Degree of Freedom Model of a Rotor Blade," *Journal of Engineering for Gas Turbines and Power,* vol. 131, pp. 012506-1 - 012506-8, 2010.

[5] C. Siewert*, et al.*, "Multiharmonic Forced Response Analysis of a Turbine Blading Coupled by Nonlinear Contact Forces," *Journal of Engineering for Gas Turbines and Power,* vol. 132, pp. 082501-1 -08501-9, 2010.

[6] J. W. Larsen and S. R. K. Nielsen, "Nonlinear Parametric Instability of Wind Turbine Wings," *Journal of Sound and Vibration,* vol. 299, pp. 64-82, 2007.

[7] I. Dobson*, et al.* (1992) Voltage Collapse in Power Systems, Circuit and System Techniques for Analyzing Voltage Collapse are Moving Toward Practical Application - and None too Soon. *IEEE Circuits and Devices Magazine*. 40-45.

[8] Q. Mu*, et al.*, "Circuit Approaches to Nonlinear-ISI Mitigation in Noise-Shaped Bandpass D/A Conversion," *IEEE Transactions on Circuits and Systems,* vol. 57, pp. 1559-1572, 2010.

[9] N. Garcia, "Periodic Steady-State Solutions of Nonlinear Circuits Based on a Differentiation Matrix," presented at the 2010 IEEE International Symposium on Circuits and Systems (ISCAS), 2010.

[10] S. R. Anderson*, et al.*, "Nonlinear Dynamic Modeling of Isometric Force Production in Primate Eye Muscle," *IEEE Transactions on Biomedical Engineering,* vol. 57, pp. 1554-1567, 2010.

[11] R. F. Ker, *et al.*, "The Spring in the Arch of the Human Foot," *Nature,* vol. 325, pp. 147-149, 1987.
[12] J. B. Dingwell and J. P. Cusumano, "Nonlinear time series analysis of normal and pathological human walking," *Chaos,* vol. 10, pp. 848-63, 2000.
[13] J. A. Nessler, *et al.*, "Nonlinear Time Series Analysis of Knee and Ankle Kinematics During Side by Side Treadmill Walking," *Chaos,* vol. 19, pp. 026104.1-026104.11, 2009.
[14] J. Duysens and H. W. A. A. Van de Crommert, "Neural Control of Locomotion; Part 1: The Central Pattern Generator from Cats to Humans," *Gait and posture,* vol. 7, pp. 131-141, 1998.
[15] A. D. Kuo, "The Relative Role of Feedforward and Feedback in the Control of Rhythmic Movements," *Motor Control,* vol. 6, pp. 129-145, 2002.
[16] M. Schultze and D. G. Thelen, "Use of a Central Pattern Generator for Control of a Muscle-Actuated Simulation of Pedaling," in *ASME 2009 Summer Bioengineering Conference (SBC2009)*, Lake Tahoe, California, USA, 2009.
[17] G. Taga, *et al.*, "Self-Organized Control of Bipedal Locomotion by Neural Oscillators in Unpredictable Environment," *Biological Cybernetics,* vol. 65, pp. 147-159, 1991.
[18] A. H. Nayfeh and D. T. Mook, *Nonlinear Oscillations*. New York: John Wiley and Sons, 1979.
[19] Z. K. Peng, *et al.*, "Comparison Between Harmonic Balance and Nonlinear Output Frequency Response Function in Nonlinear System Analysis," *Journal of Sound and Vibration,* vol. 311, pp. 56-73, 2008.
[20] A. F. Vakakis and C. Cetinkaya, "Analytical Evaluation of Periodic Responses of a Forced Nonlinear Oscillator," *Nonlinear Dynamics,* vol. 7, pp. 37-51, 1995.
[21] T. K. Caughey and A. F. Vakakis, "A Method for Examining Steady State Solutions of Forced Discrete Systems with Strong Non-Linearities," *International Journal of Non-Linear Mechanics,* vol. 26, pp. 89-103, 1991.
[22] C. Padmanabhan and R. Singh, "Analysis of Periodically Excited Non-linear Systems by a Parametric Continuation Technique," *Journal of Sound and Vibration,* vol. 184, pp. 35-58, 1995.
[23] P. Ribeiro, "Non-linear Forced Vibrations of Thin/Thick Beams and Plates by the Finite Element and Shooting Methods," *Computers and Structures,* vol. 82, pp. 1413-1423, 2004.
[24] M. Peeters, *et al.*, "Nonlinear Normal Modes, Part II: Towards a Practical Computation Using Numerical Continuation Techniques," *Mechanical Systems and Signal Processing,* vol. 23, pp. 195-216, 2009.
[25] S. M. Roberts and J. S. Shipman, *Two-Point Boundary Value Problems: Shooting Methods*. New York: American Elsevier Publishing Company, Inc., 1972.
[26] J. C. Slater, "A Numerical Method for Determining Nonlinear Normal Modes," *Nonlinear Dynamics,* vol. 10, pp. 19-30, 1996.
[27] J. C. Slater, "An Optimization Based Technique for Determining Nonlinear Normal Modes," presented at the ASME Design Engineering Devision on Active Control of Vibration and Noise, Atlanta, Georgia, USA, 1996.
[28] R. U. Seydel, *Practical Bifurcation and Stability Analysis: From Equilibrium to Chaos*, 2nd ed. New York: Springer-Verlag, 1994.
[29] E. Doedel, "Auto, Software for Continuation and Bifurcation Problems in Ordinary Differential Equations," *(http://indy.cs.concordia.ca/auto/)*.
[30] W. Govaerts, *et al.*, "MATCONT : CL_MATCONTM: A Toolbox for Continuation and Bifurcation of Cycles of Maps," *http://sourceforge.net/projects/matcont/*, 2008.
[31] J. Awrejcewicz and J. Someya, "Periodic, Quasi-Periodic and Chaotic Orbits and Their Bifurcations in a System of Coupled Oscillators," *Journal of Sound and Vibration,* vol. 146, pp. 527-532, 1991.
[32] T. C. Kim, *et al.*, "Super- and Sub-Harmonic Response Calculations for a Torsional System with Clearance Nonlinearity Using the Harmonic Balance Method," *Journal of Sound and Vibration,* vol. 281, pp. 965-993, 2005.
[33] C. Padmanabhan and R. Singh, "Dynamics of a Piecewise Non-Linear System Subject to Dual Harmonic Excitation Using Parametric Continuation," *Journal of Sound and Vibration,* vol. 184, pp. 767-799, 1995.
[34] C. Padmanabhan and R. Singh, "Analysis of Periodically Forced Nonlinear Hill's Oscillator with Application to a Geared System," *Journal of Acoustical Society of America,* vol. 99, pp. 324-334, 1996.
[35] C. Padmanabhan and R. Singh, "Influence of Mean Load on the Response of a Forced Non-Linear Hill's Oscillator," presented at the ASME Design Engineering Technical Conferences Boston, Massachusetts, 1995.
[36] G. Kerschen, Kowtko, J., McFarland, D.M., Bergman, L., Vakakis, A., "Theoretical and Experimental Study of Multimodal Targeted Energy Transfer in a System of Coupled Oscillators," *Nonlinear Dynamics,* vol. 47, pp. 285-309, 2007.
[37] G. Kerschen, Peeters, M., Golinval, J.C., Vakakis, A.F., "Nonlinear Normal Modes, Part I: A Useful Framework for the Structural Dynamicist," *Mechanical Systems and Signal Processing,* vol. 23, pp. 170-194, 2009.
[38] G. Kerschen, *et al.*, "Theoretical and Experimental Study of Multimodal Targeted Energy Transfer in a System of Coupled Oscillators," *Nonlinear Dynamics,* vol. 47, pp. 285-309, 2007.

[39] G. Kerschen*, et al.*, "Theoretical and Experimental Modal Analysis of Nonlinear Mechanical Systems, IMAC XXVIII Preconference Course," in *28th International Modal Analysis Conference (IMAC XXVIII)*, Jacksonville, Florida, USA, 2010.
[40] S. L. Lee*, et al.*, "Complicated Dynamics of a Linear Oscillator with a Light, Essentially Nonlinear Attachment," *Physica D,* vol. 204, pp. 41-69, 2005.
[41] R. Viguie*, et al.*, "Energy Transfer and Dissipation in a Duffing Oscillator Coupled to a Nonlinear Attachment," *Journal of Computational and Nonlinear Dynamics,* vol. 4, pp. 041012-1 - 041012-13, 2009.
[42] F. Georgiades*, et al.*, "Modal Analysis of a Nonlinear Periodic Structure with Cyclic Symmetry," *AIAA Journal,* vol. 47, pp. 1014-1025, 2009.
[43] J. Guckenheimer and P. Holmes, *Nonlinear Oscillations, Dynamical Systems, and Bifurcations of Vector Fields* vol. 42. New York: Springer-Verlag New York Inc., 1983.
[44] A. H. Nayfeh and B. Balachandran, *Applied Nonlinear Dynamics: Analytical, Computational and Experimental Methods*. New York: John Wiley & Sons, Inc., 1995.
[45] P. Montagnier*, et al.*, "The Control of Linear Time-Periodic Systems Using Floquet-Lyapunov Theory," *International Journal of Control,* vol. 77, pp. 472-490, 2004.
[46] M. W. Sracic and M. S. Allen, "Identifying Parameters From Nonlinear Cantilever Beams using Linear Time-Periodic Approximations," presented at the 29th International Modal Analysis Conference (IMAC XXVI), Jacksonville, Florida, USA, 2011.
[47] F. Thouverez, "Presentation of the ECL Benchmark," *Mechanical Systems and Signal Processing,* vol. 17, pp. 195-202, 2003.